



Cite this: *Phys. Chem. Chem. Phys.*,
2016, **18**, 3040

Supported lipid bilayer repair mediated by AH peptide†

Min Chul Kim,^{ab} Anders Gunnarsson,^c Seyed R. Tabaei,^{ab} Fredrik Höök^c and Nam-Joon Cho^{*abd}

The adsorption and fusion of small unilamellar lipid vesicles on silica-based substrates such as glass is a common method used to fabricate supported lipid bilayers. Successful bilayer formation depends on a number of experimental conditions as well as on the quality of the vesicle preparation. Inevitably, a small fraction of unruptured vesicles always remains in a supported bilayer, and this kind of defect can have devastating influences on the morphological and electrical properties of the supported bilayer when used as a biosensing platform. In this paper, a simple method is reported to improve the completeness of supported bilayers by adding a vesicle rupturing peptide as a final step in the fabrication process. Peptide treatment reduces the fraction of unruptured vesicles to less than 1%, as determined by epifluorescence microscopy and quartz crystal microbalance-dissipation experiments. This step can easily be incorporated into existing procedures for preparing high-quality supported lipid bilayers.

Received 24th October 2015,
Accepted 1st December 2015

DOI: 10.1039/c5cp06472d

www.rsc.org/pccp

Introduction

Formation of planar lipid bilayers on solid supports using phospholipid self-assembly is broadly utilized in scientific research as a versatile means to generate biomimetic model platforms enabling detailed studies of highly complex biological cell membranes.^{1,2} The progress made since the first discovery of the successful formation of a model membrane mimicking cell membranes¹ has opened up a large variety of applications ranging from understanding fundamental phenomena of cellular membranes to highly advanced biomedical assays, including cell culture platforms,^{3–6} biosensor development,^{3,4} drug screening^{4,5} and medical diagnostics.⁶

A large number of model membrane platforms has been explored, including the polymer cushioned lipid bilayer,^{5,7} the tethered lipid bilayer,^{8,9} the black lipid bilayer^{10,11} and the planar lipid bilayer.^{12–15} Among the options, the planar supported lipid bilayer (SLB) has gained great popularity because of its high stability and the relatively simple procedures by which it can be formed.^{12,15} SLBs are typically produced by either Langmuir–Blodgett (LB) deposition,¹⁶ the solvent

assisted lipid bilayer formation method^{17–22} or surface mediated vesicle fusion.²³ While LB deposition requires advanced equipment and several steps to sequentially transfer lipid monolayers to the solid substrate, the vesicle fusion method simply utilizes vesicle adsorption, followed by spontaneous rupture when a critical vesicle coverage has been reached on certain hydrophilic substrates including mica, glass or other silica-based surfaces.²⁴ For the vesicle fusion method, the pathways to cause vesicle rupture-forming lipid bilayers on solid supports are complex, and representative parameters responsible for vesicle fusion and rupture are numerous and include vesicle size,²² lipid composition,²⁵ osmotic pressure,²⁶ ionic strength,²⁷ temperature,²⁸ solution pH²⁹ and the presence of divalent cations.³⁰

Based on the previously mentioned parameters, the interactions between lipid vesicles and solid supports can be tuned in order to promote or inhibit vesicle rupture leading to SLB formation. Nonetheless, the quality of the SLB with respect to defect density, lateral mobility and the remaining number of non-ruptured vesicles may vary not only from situation to situation but also when attempts are made to perfectly reproduce identical experimental conditions. The imperfections may create significant fractions of inhomogeneity within the bilayer, which may in turn produce short circuits interrupting the measurement of electrical properties of membrane bound channels³¹ and also create artifacts when conducting fluorescence-based bilayer related assays.

In this paper, a simple method is presented to improve the completeness of supported lipid bilayers through a repair step that is aided by the capacity of an amphiphatic

^a School of Materials Science and Engineering, Nanyang Technological University, 50 Nanyang Avenue 639798, Singapore. E-mail: njcho@ntu.edu.sg

^b Centre for Biomimetic Sensor Science, Nanyang Technological University, 50 Nanyang Drive 637553, Singapore

^c Department of Applied Physics, Chalmers University of Technology, Gothenburg, Sweden

^d School of Chemical and Biomedical Engineering, Nanyang Technological University, 62 Nanyang Drive 637459, Singapore

† Electronic supplementary information (ESI) available. See DOI: 10.1039/c5cp06472d

α -helical (AH) peptide to induce vesicle rupture.^{32–34} In a series of publications^{20,33–38} from our groups and others, the capacity of this AH peptide to promote SLB formation has been explored, in particular on substrates^{32,33–36} and lipid compositions^{15,34,37,38} that are not compatible with vesicle adsorption induced SLB formation.^{15,34,37,38} For example, Hardy *et al.* succeeded in employing the AH peptide to rupture HIV lipid envelope-mimicking vesicles into SLBs containing high fractions of cholesterol,³⁹ and recently extended this research by exploring concentration-dependent behaviors of SLB–peptide interactions using atomic force microscopy.⁴⁰ It has also been shown that using a tethered unilamellar vesicle assay with single vesicle resolution, 100 nM of AH peptide caused single zwitterionic lipid vesicles to rupture at rates that were inversely related to the vesicle diameter^{41–43} and similar vesicle rupture behavior was also observed with another related peptide analogue.³⁸ Inspired by these reports, in this work the possibility of using the AH peptide to repair inevitably occurring imperfections in SLBs generated using the vesicle fusion method has been explored. The AH peptide controlled SLB repair process was investigated using the quartz crystal microbalance with dissipation (QCM-D) monitoring and epifluorescence microscopy techniques. Particular emphasis was put on exploring the possibility of generating high quality and completely supported lipid bilayers utilizing lipid vesicles with increasing geometrical dimensions. This new repair method is anticipated to provide an attractive tool towards creating a defect free, supported lipid bilayer as a broad platform for various bioanalytical applications.

Materials and methods

Vesicle preparation

Various populations of lipid vesicles composed of 1-palmitoyl-2-oleoyl-*sn*-glycero-3-phosphocholine (POPC) lipid (Avanti Polar Lipids, Alabaster, AL) were prepared by the extrusion method.⁴⁴ Vesicles were extruded by using a Mini-Extruder (Avanti Polar Lipids) through track-etched polycarbonate membranes (Whatman Schleicher & Schuell, Dassel, Germany) with pores ranging from 50 to 400 nm diameter. POPC lipids dissolved in chloroform were dried under a gentle stream of nitrogen gas and kept under vacuum to remove any remaining chloroform residue. To create various sizes of unilamellar vesicles, the vesicles were passed through the different sized pore membranes between 7 to 27 times by using the Mini-Extruder. Each vesicle suspension was diluted to 0.2 mg mL⁻¹ before use. An aqueous buffer solution of 150 mM sodium chloride (NaCl) and 10 mM Tris in 18.2 M Ω cm Milli-Q treated water (Millipore, Billerica, MA) at pH 7.5 was used in all measurements.

Peptide reagent

The AH peptide was synthesized by AnaSpec Inc., (San Jose, CA). The sequence of the AH peptide is H-Ser-Gly-Ser-Trp-Leu-Arg-Asp-Val-Trp-Asp-Trp-Ile-Cys-Thr-Val-Leu-Thr-Asp-Phe-Lys-Thr-Trp-Leu-Gln-Ser-Lys-Leu-Asp-Tyr-Lys-Asp-NH₂. The peptide was prepared and diluted in Tris buffer before the measurements.

Dynamic light scattering

Dynamic light scattering measurements were conducted on a NanoBrook 90Plus particle size analyzer (Brookhaven Instruments Corporation, Holtsville, NY) with a 658.0 nm monochromatic laser to measure size distributions of extruded vesicles. Every measurement was taken at a scattering angle of 90° at 25 °C. The light scattering data were collected using digital autocorrelator software (Brookhaven Instruments Corporation). In order to check for multi-modal distributions and to calculate the intensity weighted Gaussian profile of various size distributions including average effective diameter and polydispersity, all autocorrelation functions acquired were analyzed by CONTIN and non-negatively constrained least squares algorithms. Size distributions of each vesicle size are presented in Fig. S2 (ESI†).

Quartz crystal microbalance-dissipation measurements

Adsorption kinetics and properties of the adsorbed layer were monitored using the QCM-D technique with a Q-Sense E4 instrument (Q-Sense AB, Gothenburg). In QCM-D experiments, the resonance frequency and energy dissipation of the quartz crystal can be obtained simultaneously.¹⁵ Silicon oxide (SiO₂) coated QCM crystal sensor chips (AT-cut quartz crystals, Q-Sense) were used for each measurement. Before the experiment, the crystals were treated with oxygen plasma using a plasma cleaner (Harrick Plasma, Ithaca, NY) at 80 W for 5 min. Experimental data were measured at various overtones ($n = 3, 5, 7, 9$ and 11), and corresponding changes in resonance frequency and energy dissipation were monitored. The obtained experimental data from the third to seventh overtones were fitted to the Sauerbrey model in order to calculate the effective thickness of the adsorbed layer.³⁶

Epifluorescence microscopy

Epifluorescence imaging of supported lipid bilayers formed on a glass substrate was done with an inverted Eclipse Ti-U optical microscope (Nikon, Japan). Imaging was done by using a 60 \times magnification (Numerical aperture (NA) = 1.49) oil immersion objective (Nikon) for measurements resulting in a camera pixel size of 0.267 \times 0.267 μ m. An iXon 512 \times 512 pixel electron multiplying charge-coupled device camera (Andor Technology, Belfast) was used to capture the fluorescence images, and a fiber-coupled mercury lamp (Intensilight C-HGFIE; Nikon) was used to excite the fluorophores. A tetramethylrhodamine isothiocyanate filter was used to filter out the excitation light and the emission light from the measurements with rhodamine-polyethylene (Rh-PE) fluorophores.

Fluorescence recovery after photobleaching (FRAP)

To conduct fluorescence recovery after photobleaching (FRAP) measurements, a circular spot of 20 μ m diameter was photobleached for 5 s using a 532 nm, 100 mW laser (Klaser Technologies, Dortmund). Fluorescence micrographs were imaged for 90 s at 1 s intervals, and the corresponding lateral

diffusion coefficients were obtained based on the Hankel transform method.⁴⁵

Results and discussion

The mechanism of vesicle fusion includes a complex sequence of steps involving vesicle adsorption, deformation, fusion, and rupture leading to reassembly that may eventually result in SLB formation (Fig. 1A and Fig. S1, ESI†). Fig. 1B presents a typical fluorescence micrograph of a good quality SLB (Fig. S1C, ESI†).

However, even under optimal fabrication conditions, it is our experience that there always remains a number of unruptured or entrapped vesicles in the SLB, which can be easily visualized using epi- or total internal reflection-fluorescence microscopy measurements,⁴⁶ as illustrated in Fig. 1C–E. Upon SLB formation on silica using vesicles with a mean diameter of approximately 91 nm composed of POPC lipid, a significant number (1000 per $136 \times 136 \mu\text{m}^2$) of unruptured vesicles also remained bound after extensive rinsing, either in Tris buffer or in deionized water, of which the latter induces a large osmotic pressure

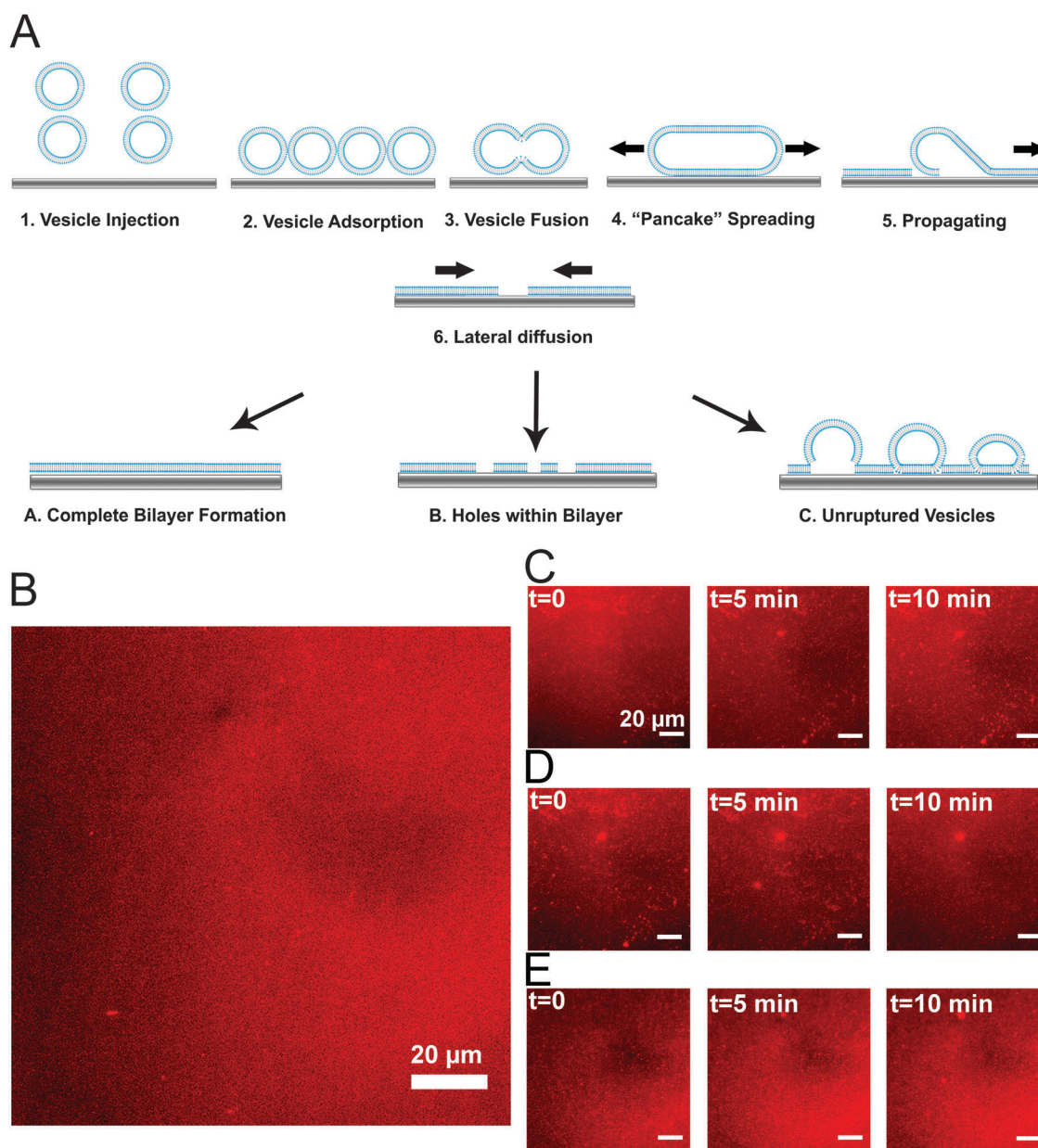


Fig. 1 Formation of a SLB on glass substrate and its experimental defective cases. Schematics of (A) an overall process of SLB formation via a vesicle fusion method on the glass substrate and its possible results after the critical vesicle rupture and following washing with buffer. A supported lipid bilayer was formed on a glass substrate via a vesicle fusion method using 30 nm sized membrane filtered lipid vesicles. Here are presented good and defective cases of planar lipid bilayer fluorescence images, (B) complete lipid bilayer and (C–E) unruptured vesicles trapped on bilayers. After the rupture of the adsorbed vesicles, the lipid bilayer was washed with three different solvents, (C) initial Tris buffer (10 mM Tris, 150 mM NaCl and pH 7.5), (D) Milli-Q water and (E) Tris buffer (10 mM Tris, 1 M NaCl and pH 7.5). Note that fluorescence image traces of each washing process were collected for 15 minutes. Each scale bar represents 20 μm .

difference that could tentatively aid vesicle removal and SLB repair²⁶ (Fig. 1C and D). The limited effect obtained by rinsing in deionized water highlights that incomplete rupture or imperfect formation of SLB is common not only when there are large unruptured vesicles,⁴⁷ but also when SLBs are formed using small vesicles (diameter less than 100 nm, see Fig. S2, ESI,† for vesicle size distribution) because of the steric effect in saturated adlayers. Thus, a post-assembly repair method that could aid the formation of defect free SLBs would be highly desirable.

Repair of unruptured trapped vesicles within SLBs

Based on the previously mentioned studies,^{15,33–35,37,38,41} it may be possible to rupture the bound vesicles trapped on the initially formed lipid bilayer by an AH peptide. Previously a mechanism was proposed for AH peptide mediated transformation of intact vesicles into a SLB by using simultaneous QCM-D and optical reflectometry measurements.³³ Using the combined techniques, the time-dependent variation could be monitored in adsorbed molecular mass (optical mass), adsorbed molecular mass and solvent mass (acoustic mass), effective thickness, and effective reflective index of the lipid adlayer during the course of the AH peptide interaction with surface adsorbed lipid vesicles. Briefly, the process of AH peptide induced vesicle to bilayer transformation comprises three steps: (1) AH peptide binding to vesicles, (2) swelling of vesicles, (3) desorption of AH peptide and lipids resulting in formation of an adlayer with a thickness of ~ 5.1 nm and an effective refractive index of ~ 1.45 , and these results are in very good agreement with the expected values for a lipid bilayer. In order to explore this possibility, the QCM-D technique was utilized for tracking the kinetic changes upon addition of AH peptide and subsequent interaction with trapped unruptured vesicles. To obtain a sufficient number of unruptured vesicles trapped on and within the bilayer, large vesicles (~ 220 nm) were intentionally fabricated for substrate

deposition as shown in Fig. 2A and B. Upon injection of large size vesicles onto the SiO₂ substrate, two-step kinetics²⁵ were typically observed, which were indicative of reaching a critical surface coverage of adsorbed vesicles before the fusion and rupture processes were initiated. However, during the latter process, vesicles were continuously adsorbed onto the substrate, which is shown by the frequency decrease and dissipation increase after the first peak. Upon subsequent injections of Tris buffer, the frequency shift increased from -65.3 Hz to -37 Hz and the energy dissipation shift decreased from 12.2 to 4.0×10^{-6} (Fig. 2A and B), demonstrating suppressed vesicle adsorption and that a significant fraction of adsorbed unruptured vesicles were rinsed off. Nevertheless, the final changes in Δf and ΔD still deviated significantly from those corresponding to a complete SLB ($\Delta f \sim 26$ Hz and $\Delta D \sim 0 \times 10^{-6}$),¹⁵ which indicates that a significant fraction of unruptured vesicles remained entrapped on the bilayer. To independently verify this conjecture, epifluorescence microscopy was used to visualize unruptured vesicles, which were clearly visible as bright dots surrounded by a uniform lipid bilayer (Fig. 1C–E). Taking the contribution to the frequency shift originating from coupled water into account,⁴⁸ the vesicle coverage estimated by the two methods are in good agreement with each other.

In order to promote complete SLB formation or repair the defects, $8 \mu\text{M}$ AH peptide were added to the bilayer, and time sequence fluorescence micrographs were captured as shown in Fig. 2D. In addition, as a result of the peptide injection (see arrow 3 in Fig. 2A and B), the saturated QCM-D response upon peptide injection corresponded to the responses expected for a complete SLB,²⁴ *i.e.*, $\Delta f \sim -26$ Hz and $\Delta D \sim 0 \times 10^{-6}$ (Fig. 2A and B). In order to further characterize the properties of the resulting adlayer, the Sauerbrey model³⁶ was applied to compute the effective thickness of the adlayer. For the calculations, 1000 kg m^{-3} was assumed as the density of the adlayer.³⁶ The Sauerbrey thickness for the different overtones reached saturation

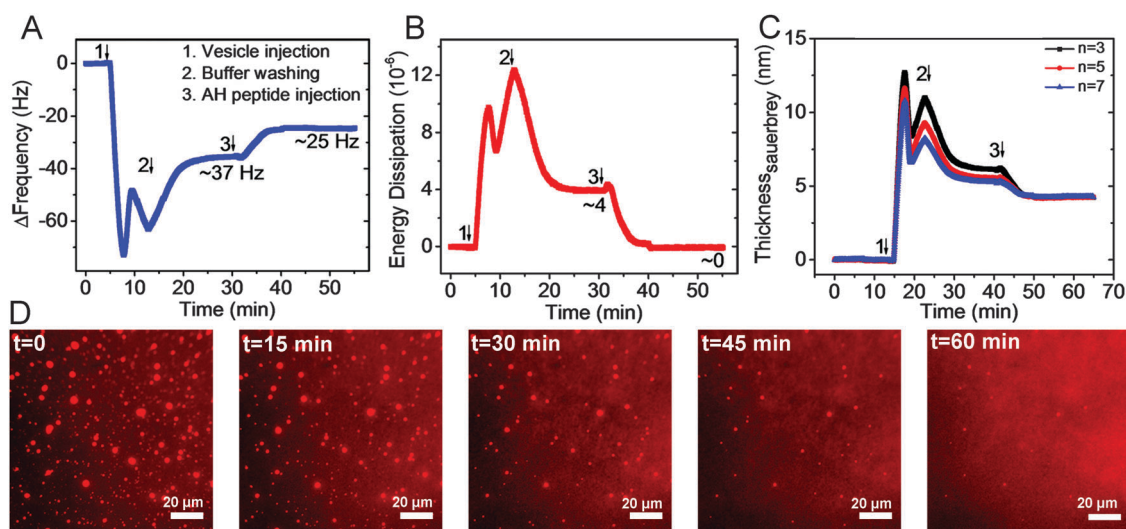


Fig. 2 SLB formation and its repair mediated by AH peptide. After the vesicle (diameter ~ 222.1 nm) adsorption, initial rupture and AH peptide injection, changes in (A) resonant frequency and (B) energy dissipation were monitored. (C) Sauerbrey thickness of the adlayer. $n = 3$ (black line), $n = 5$ (red line), and $n = 7$ (blue line) overtones. (D) Time-lapse fluorescence micrographs of AH peptide mediated SLB repair formed by 188 nm diameter lipid vesicles. Scale bars are $20 \mu\text{m}$.

at ~ 12.7 , ~ 10.9 , and ~ 6.2 nm (Fig. 2C). As a result of AH peptide mediated repair, the resulting thickness of the SLB obtained from the Sauerbrey model was ~ 4.2 nm indicating that a complete SLB is formed with the aid of AH peptide.

Furthermore, to confirm the successful repair, the process of AH peptide mediated rupturing of the remaining vesicles was visualized using a small fraction (0.5 mol%) of Rh-labeled lipid vesicles imaged using epifluorescence microscopy, as shown in time sequence micrographs (Fig. 2C). The AH peptide was injected after the vesicle fusion of large size vesicles (approximately ~ 188 nm diameter) and a subsequent buffer washing step. The micrographs presented show time-lapsed images after AH peptide injection. After peptide injection, a vast majority of trapped vesicles were ruptured, signaling efficient repair of the SLB. The epifluorescence images were captured for a total of ~ 50 min after the injection and each frame of the sequential micrographs is shown at an interval of ~ 5.6 min. Note that there is a large deviation in time scales between that of the QCM-D kinetic profiles and epifluorescence imaging, which is attributed to the different measurement chamber geometries and corresponding flow conditions and possibly also the different substrates (glass *versus* sputtered SiO_2).

To confirm the retention of lateral diffusivity after AH peptide addition, FRAP measurements were conducted before and after the repair as shown in Fig. 3. It was confirmed that lipid mobility was still retained with a moderate drop of the diffusion coefficient from $\sim 2.3 \mu\text{m}^2 \text{s}^{-1}$ to $\sim 0.9 \mu\text{m}^2 \text{s}^{-1}$, but still displayed a mobile fraction of 89% as shown in Fig. 3B. The decrease in lateral diffusivity of the SLB is likely to be because of a small fraction of bound AH peptide.³⁵

As a final verification of the repair process, an AH peptide treated zwitterionic SLB was investigated to see if it remained resistant to nonspecific adsorption of bovine serum albumin (BSA).⁴⁹ Because BSA protein binding was not detectable using the QCM-D technique, epifluorescence microscopy with a sensitivity which was orders of magnitude higher was used to

probe the binding of fluorescently labeled BSA upon addition to the SLB either without or with prior AH peptide treatment and the amount bound was quantified using the fluorescence intensity per unit area (Fig. S3A, ESI[†]). In both cases, protein adsorption was minimal and is consistent with AH peptide mediated vesicle rupture leading to localized SLB formation, which in turn improves the completeness of the SLB platform as a whole. As a control, BSA adsorption onto a bare glass substrate was also tested and, as expected, there was a significantly larger amount of adsorbed protein. There was a greater than 30-fold reduction in adsorbed proteins to the SLBs *versus* the glass substrate, verifying that AH peptide treatment preserves the anti-biofouling properties of zwitterionic SLBs (Fig. S3B, ESI[†]). The collective set of measurement data indicates that AH peptide mediated SLB repair acts by converting adsorbed, unruptured vesicles into SLB fragments that fill in the defect sites (*i.e.*, the sites of previously unruptured vesicles), leading to a complete and homogenous SLB platform.

Vesicle size dependent SLB formation and repair

The repair ability of the AH peptide was further tested for SLB formed using a broad range of lipid vesicle sizes ranging from ~ 90 to ~ 800 nm. Smaller vesicles with a diameter less than 100 nm were previously demonstrated to rupture and form an essentially complete bilayer whereas larger vesicles tend to form mixed layers of SLB fragments with a high number of entrapped vesicles.²⁴ Here, the attention was focused on addition of AH peptide after vesicle adsorption and monitored the corresponding changes in the kinetics of vesicle rupture upon the addition of AH peptide for different vesicle sizes. In order to explore in detail the effects of differently sized vesicles on AH peptide mediated repair, adsorption kinetic profiles from QCM-D measurements were set to zero after the initial vesicle adsorption and fusion step and subsequent rinsing in buffer (Fig. 4). It was shown that the kinetics of AH peptide mediated repairing occurs in a vesicle size dependent manner, displaying a trend in terms

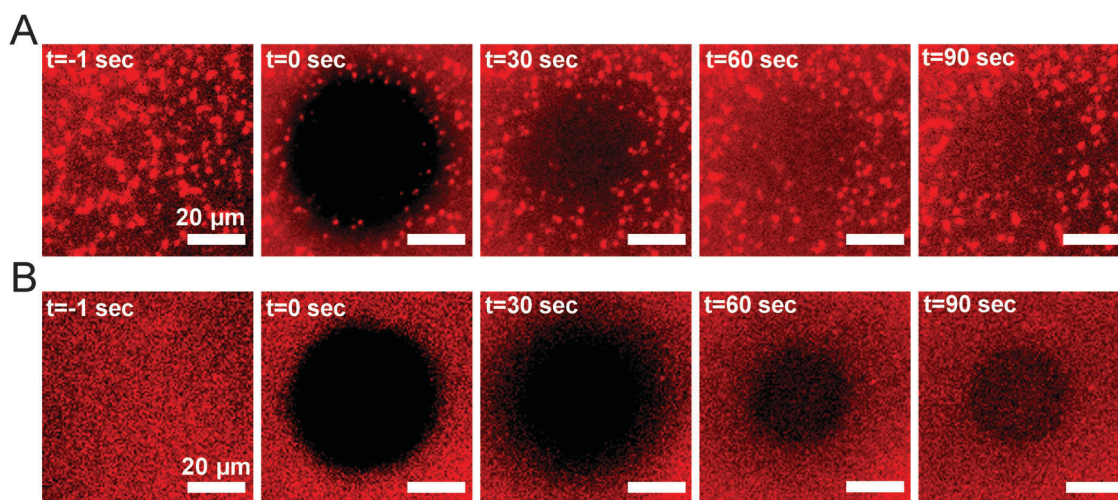


Fig. 3 FRAP micrographs of SLB showing pre- and post-repair by the AH peptide. Each post-bleaching micrograph is shown at 30 s intervals. Scale bar represents 10 μm .

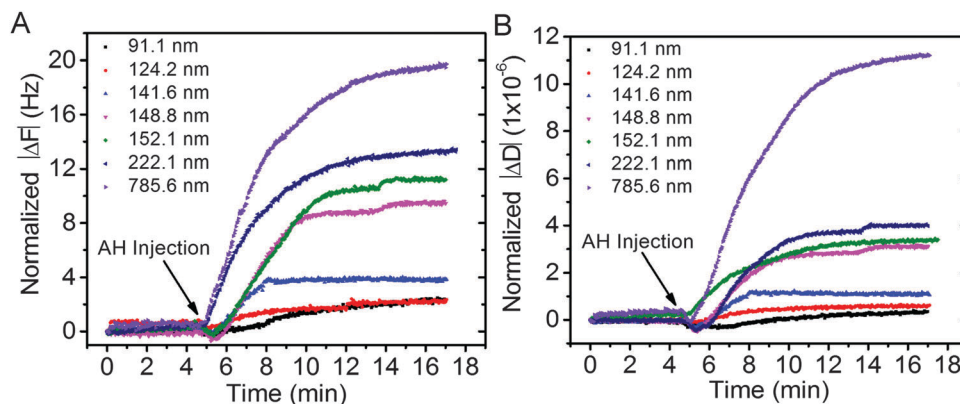


Fig. 4 Influence of vesicle size on AH peptide mediated SLB repair. Kinetic profiles of repair on various sizes of vesicles were monitored using QCM-D. After the rupture of each different sized vesicle, (A) changes in resonant frequency and (B) energy dissipation at the third overtone were normalized at $t = 0$ min. Arrows indicate injection of AH peptide.

Table 1 Summary of results obtained for SLB repair mediated by AH peptide. Initial/final changes in resonance frequency and energy dissipation at the third overtone before and after the repair are reported as a function of extrusion filter size. Note that each subscript value 1 indicates before the repair, while the subscript value 2 corresponds to the final kinetic values after the repair. The numbers with an asterisk indicate how many times vesicle containing solutions were passed through the extrusion membrane filters

Extrusion filter size (nm)	DLS measurement size (nm)	Polydispersity	ΔF_1 (Hz)	ΔF_2 (Hz)	ΔD_1 (1×10^{-6})	ΔD_2 (1×10^{-6})
50 (23*)	91.0 ± 0.2	0.079	28.78	26.37	0.5122	0.1576
100 (23*)	128.7 ± 0.7	0.058	28.82	26.34	0.5836	0.0137
100 (17*)	141.3 ± 0.7	0.078	29.75	26.13	1.0941	0.0126
100 (13*)	148.5 ± 0.6	0.092	37.01	27.63	3.2182	0.1286
100 (7*)	151.8 ± 1.2	0.093	38.39	27.00	3.5131	0.2933
200 (13*)	221.3 ± 1.4	0.173	37.16	25.00	4.0272	0.0127
400 (7*)	784.9 ± 12.9	0.347	46.34	26.25	11.4280	0.0469

of Δf and ΔD increasing from ~ 2.4 to ~ 20 Hz and $\sim 0.3 \times 10^{-6}$ to $\sim 11 \times 10^{-6}$, respectively, for vesicles increasing in size from approximately 91.1 nm to 785.6 nm (Fig. 4 and Table 1). The trend of increasing frequency and dissipation shifts with larger vesicle sizes is attributed to both the number of unruptured vesicles which tends to increase with vesicle size as well as the size of individual vesicles which leads to a greater response per vesicle upon AH peptide mediated rupture. Indeed, the measurement signatures are interpreted as a direct consequence of

efficient AH peptide induced rupture of vesicles trapped in the SLB formed initially. Thus, it was demonstrated that the AH peptide can act as a broadly applicable repair agent of trapped vesicles even in unfavorable conditions for SLB formation.

SLB repair pathway

To gain further insight into the repair process, the vesicle size dependent repair mediated by AH peptide was imaged (Fig. 5A–C and Movies S1–S3, ESI[†]), and the corresponding numbers of

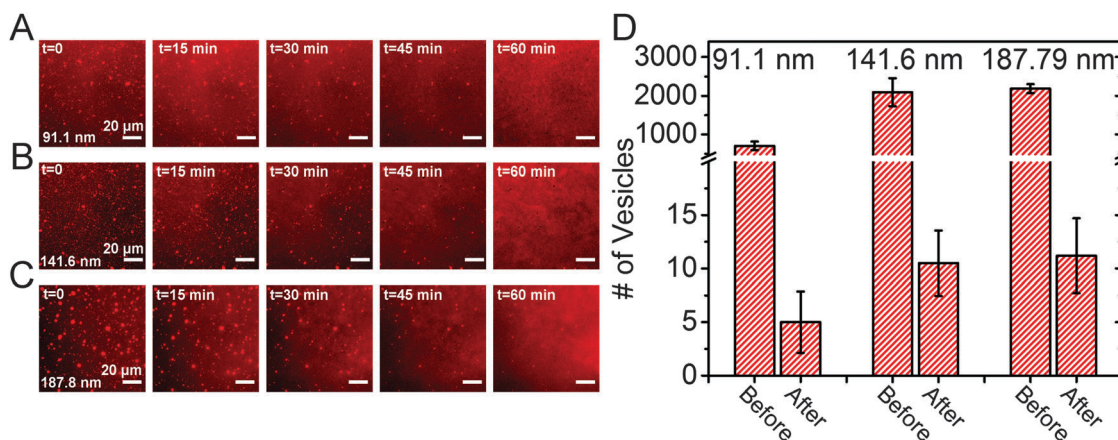


Fig. 5 Time-lapse fluorescence micrographs of AH peptide mediated SLB repair. (A–C) Fluorescence micrographs of bilayer repair process as a function of vesicle size. Scale bars are 20 μm . (D) Number of unruptured vesicles before and after AH peptide treatment.

unruptured vesicles before and after repair were estimated based on a fluorescence threshold (Fig. 5D). Three different SLBs formed using various sizes of vesicles showed distinctive characteristics. For the case of ~ 90 nm (Fig. 5A), a much lower number of unruptured vesicles was observed compared to the other bilayers formed using larger sizes of vesicles. This is consistent with previously reported findings that smaller vesicles easily rupture to form a relatively complete bilayer, while larger vesicles tend to form a mixed layer of SLB and intact vesicles.⁴⁷ Regardless of the size of vesicles used to form the bilayer, all three cases investigated (91.1, 141.6 and 187.79 nm) resulted in less than ~ 10 unruptured or trapped vesicles per field of view ($136 \times 136 \mu\text{m}^2$) on the bilayer after treatment with AH peptide. From the fluorescence micrographs, features signaling a structural transformation of the intact vesicles upon binding with AH peptide were observed (see Movies S1-S3, ESI[†]). This experimental finding supports the previously reported mechanism³² that vesicle rupture mediated by AH peptide is caused by expansion/swelling of intact vesicles, which was observed here to include creation of microvilli or finger-like structures on the outer leaflet of the vesicles. The kinetic profiles from QCM-D measurements (*cf.* Fig. 2A and 4A) are consistent with a structural transformation, although structural details cannot be revealed from ensemble averaging data alone.

Conclusions

Collectively, the experimental findings and analytical results presented here demonstrate a post-assembly repair process mediated by AH peptide allowing the generation of a complete and homogenous SLB with somewhat reduced, but still retained, lateral fluidity. This is the first report in which the AH peptide is reported to repair defects on SLB formed *via* vesicle fusion, demonstrating complete SLBs with a negligible amount of unruptured vesicles. This method can be applied to form SLBs using large size vesicles, which typically cause steric hindrance that disrupts complete rupture of absorbed vesicles. Although further electrical measurements are needed in order to evaluate the insulating properties of AH peptide treated bilayers, this new SLB repair approach can improve the feasibility of SLB as a biosensor platform, particularly in cases where high quality SLBs are needed. It might also be an interesting way to form planar SLB from native cell membranes, which attracts increased use in membrane-protein chromatography applications.

Acknowledgements

The authors wish to acknowledge support from the National Research Foundation (NRF-NRFF2011-01 and NRF2015NRF-POC0001-19) and the Swedish Research Council.

References

- 1 E. Sackmann, *Science*, 1996, **271**, 43–48.
- 2 Y. H. Chan and S. G. Boxer, *Curr. Opin. Chem. Biol.*, 2007, **11**, 581–587.
- 3 H. Jung, A. D. Robison and P. S. Cremer, *J. Am. Chem. Soc.*, 2009, **131**, 1006–1014.
- 4 J. H. Jeong, J.-H. Choi, M. C. Kim, J. H. Park, J. S. Herrin, S. H. Kim, H. Lee and N.-J. Cho, *Eur. Biophys. J.*, 2015, 1–9.
- 5 M. L. Wagner and L. K. Tamm, *Biophys. J.*, 2001, **81**, 266–275.
- 6 S. Yorulmaz, S. R. Tabaei, M. Kim, J. Seo, W. Hunziker, J. Szebeni and N.-J. Cho, *Eur. J. Nanomed.*, 2015, **7**, 245–255.
- 7 J. C. Munro and C. W. Frank, *Langmuir*, 2004, **20**, 10567–10575.
- 8 O. Purrucker, A. Förtig, R. Jordan and M. Tanaka, *ChemPhysChem*, 2004, **5**, 327–335.
- 9 J. A. Jackman, W. Knoll and N.-J. Cho, *Materials*, 2012, **5**, 2637–2657.
- 10 W. Römer and C. Steinem, *Biophys. J.*, 2004, **86**, 955–965.
- 11 D. Weiskopf, E. K. Schmitt, M. H. Klühr, S. K. Dertinger and C. Steinem, *Langmuir*, 2007, **23**, 9134–9139.
- 12 P. S. Cremer and S. G. Boxer, *J. Phys. Chem. B*, 1999, **103**, 2554–2559.
- 13 I. Reviakine and A. Brisson, *Langmuir*, 2000, **16**, 1806–1815.
- 14 T. H. Anderson, Y. Min, K. L. Weirich, H. Zeng, D. Fygenon and J. N. Israelachvili, *Langmuir*, 2009, **25**, 6997–7005.
- 15 N. J. Cho, C. W. Frank, B. Kasemo and F. Höök, *Nat. Protoc.*, 2010, **5**, 1096–1106.
- 16 N. Vila, M. Puggelli and G. Gabrielli, *Colloids Surf., A*, 1996, **119**, 95–104.
- 17 S. R. Tabaei, J.-H. Choi, G. Haw Zan, V. P. Zhdanov and N.-J. Cho, *Langmuir*, 2014, **30**, 10363–10373.
- 18 S. R. Tabaei, J. A. Jackman, S.-O. Kim, B. Liedberg, W. Knoll, A. N. Parikh and N.-J. Cho, *Langmuir*, 2014, **30**, 13345–13352.
- 19 S. R. Tabaei, S. Vafaei and N.-J. Cho, *Phys. Chem. Chem. Phys.*, 2015, **17**, 11546–11552.
- 20 J. A. Jackman, S. R. Tabaei, Z. Zhao, S. Yorulmaz and N.-J. Cho, *ACS Appl. Mater. Interfaces*, 2015, **7**, 959–968.
- 21 S. R. Tabaei, J. A. Jackman, S.-O. Kim, V. P. Zhdanov and N.-J. Cho, *Langmuir*, 2015, **31**, 3125–3134.
- 22 S. R. Tabaei, J. A. Jackman, B. Liedberg, A. N. Parikh and N.-J. Cho, *J. Am. Chem. Soc.*, 2014, **136**, 16962–16965.
- 23 L. K. Tamm and H. M. McConnell, *Biophys. J.*, 1985, **47**, 105–113.
- 24 C. Keller and B. Kasemo, *Biophys. J.*, 1998, **75**, 1397–1402.
- 25 J. A. Jackman, N.-J. Cho, R. S. Duran and C. W. Frank, *Langmuir*, 2009, **26**, 4103–4112.
- 26 J. A. Jackman, J.-H. Choi, V. P. Zhdanov and N.-J. Cho, *Langmuir*, 2013, **29**, 11375–11384.
- 27 S. Boudard, B. Seantier, C. Breffa, G. Decher and O. Felix, *Thin Solid Films*, 2006, **495**, 246–251.
- 28 E. Reimhult, F. Höök and B. Kasemo, *Phys. Rev. E: Stat., Nonlinear, Soft Matter Phys.*, 2002, **66**, 051905.
- 29 N.-J. Cho, J. A. Jackman, M. Liu and C. W. Frank, *Langmuir*, 2011, **27**, 3739–3748.
- 30 B. Seantier and B. Kasemo, *Langmuir*, 2009, **25**, 5767–5772.
- 31 S. Terrettaz, M. Mayer and H. Vogel, *Langmuir*, 2003, **19**, 5567–5569.
- 32 N.-J. Cho, S.-J. Cho, K. H. Cheong, J. S. Glenn and C. W. Frank, *J. Am. Chem. Soc.*, 2007, **129**, 10050–10051.

- 33 N.-J. Cho, G. Wang, M. Edvardsson, J. S. Glenn, F. Hook and C. W. Frank, *Anal. Chem.*, 2009, **81**, 4752–4761.
- 34 G. H. Zan, J. A. Jackman and N.-J. Cho, *J. Phys. Chem. B*, 2014, **118**, 3616–3621.
- 35 N.-J. Cho, S.-J. Cho, J. O. Hardesty, J. S. Glenn and C. W. Frank, *Langmuir*, 2007, **23**, 10855–10863.
- 36 N.-J. Cho, K. K. Kanazawa, J. S. Glenn and C. W. Frank, *Anal. Chem.*, 2007, **79**, 7027–7035.
- 37 J. A. Jackman, G. H. Zan, V. P. Zhdanov and N.-J. Cho, *J. Phys. Chem. B*, 2013, **117**, 16117–16128.
- 38 G. H. Zan and N.-J. Cho, *Colloids Surf., B*, 2014, **121**, 340–346.
- 39 G. J. Hardy, R. Nayak, S. M. Alam, J. G. Shapter, F. Heinrich and S. Zauscher, *J. Mater. Chem.*, 2012, **22**, 19506–19513.
- 40 J. Wang, K.-W. Liu and S. L. Biswal, *Anal. Chem.*, 2014, **86**, 10084–10090.
- 41 S. R. Tabaei, M. Rabe, V. P. Zhdanov, N.-J. Cho and F. Höök, *Nano Lett.*, 2012, **12**, 5719–5725.
- 42 N.-J. Cho, H. Dvory-Sobol, A. Xiong, S.-J. Cho, C. W. Frank and J. S. Glenn, *ACS Chem. Biol.*, 2009, **4**, 1061–1067.
- 43 J. A. Jackman, R. Saravanan, Y. Zhang, S. R. Tabaei and N. J. Cho, *Small*, 2015, **11**, 2372–2379.
- 44 R. C. MacDonald, R. I. MacDonald, B. P. M. Menco, K. Takeshita, N. K. Subbarao and L.-R. Hu, *Biochim. Biophys. Acta, Biomembr.*, 1991, **1061**, 297–303.
- 45 P. Jönsson, M. P. Jonsson, J. O. Tegenfeldt and F. Höök, *Biophys. J.*, 2008, **95**, 5334–5348.
- 46 R. P. Richter, R. Bérat and A. R. Brisson, *Langmuir*, 2006, **22**, 3497–3505.
- 47 E. Reimhult, F. Höök and B. Kasemo, *Langmuir*, 2003, **19**, 1681–1691.
- 48 P. Bingen, G. Wang, N. F. Steinmetz, M. Rodahl and R. P. Richter, *Anal. Chem.*, 2008, **80**, 8880–8890.
- 49 K. Glasmästar, C. Larsson, F. Höök and B. Kasemo, *J. Colloid Interface Sci.*, 2002, **246**, 40–47.